ARTICLE

Structural Characterization Combined with the First Principles Simulations of Barium/Strontium Cobaltite/Ferrite as Promising Material for Solid Oxide Fuel Cells Cathodes and High-Temperature Oxygen Permeation Membranes

Shruba Gangopadhayay,[†,‡] Talgat Inerbaev,[†,§] Artëm E. Masunov,[*,†,‡,∥] Deanna Altilio,[⊥] and Nina Orlovskaya[*,⊥]

Nanoscience Technology Center, Institute for Simulation and Training, and Departments of Chemistry, Physics, and Mechanical, Materials and Aerospace Engineering, University of Central Florida, Orlando, Florida 32826

ABSTRACT Mixed ionic-electronic conducting perovskite type oxides with a general formula ABO_3 (where A = Ba, Sr, Ca and B = Co, Fe, Mn) often have high mobility of the oxygen vacancies and exhibit strong ionic conductivity. They are key materials that find use in several energy related applications, including solid oxide fuel cell (SOFC), sensors, oxygen separation membranes, and catalysts. Barium/strontium cobaltite/ferrite (BSCF) $Ba_{0.5}Sr_{0.5}Co_{0.8}Fe_{0.2}O_{3-\delta}$ was recently identified as a promising candidate for cathode material in intermediate temperature SOFCs. In this work, we perform experimental and theoretical study of the local atomic structure of BSFC. Micro-Raman spectroscopy was performed to characterize the vibrational properties of BSCF. The Jahn−Teller distortion of octahedral coordination around Co^{4+} cations was observed experimentally and explained theoretically. Different cations and oxygen vacancies ordering are examined using plane wave pseudopotential density functional theory. We find that cations are completely disordered, whereas oxygen vacancies exhibit a strong trend for aggregation in L-shaped trimer and square tetramer structure. On the basis of our results, we suggest a new explanation for BSCF phase stability. Instead of linear vacancy ordering, which must take place before the phase transition into brownmillerite structure, the oxygen vacancies in BSCF prefer to form the finite clusters and preserve the disordered cubic structure. This structural feature could be found only in the first-principles simulations and can not be explained by the effect of the ionic radii alone.

KEYWORDS: Perovskite structure • vacancy ordering • intermediate spin state • density functional theory • Jahn−Teller distortion

1. INTRODUCTION

Recent worldwide interest in cleaner energy technology has refocused attention to the solid oxide fuel cells (SOFC) as a potential source of efficient, environmentally friendly, and fuel versatile electric power. Because of high operating temperatures, the SOFCs offer several potential advantages over proton exchange membranes fuel cells including low internal resistance, high tolerance to catalyst poisons, production of high-quality waste heat for reformation of hydrocarbon fuels, as well as the possibility of oxidation of hydrocarbon fuels directly. SOFC's efficiency ranges from 50 to 65% and they can be used as environmentally acceptable source of electric energy (1, 2).

Continuous effort in the design of SOFC multicell stacks and systems requires deeper understanding of the structure/property-performance relationships. Numerous attempts had been made to explore new electrode materials and microstructures, and establish how and why electrode performance changes with time, temperature, thermal cycling, operating conditions, impurities, and other factors (1, 2). Despite the advances in electrochemical measurement and modeling, understanding of SOFC cathode oxygen reduction and transport mechanisms remains largely circumstantial today. The elucidation of the cathode mechanisms often relies on having limited understanding for an observed phenomenon (e.g., chemical capacitance as evidence for bulk transport) rather than direct independent measurements (2). Therefore, direct experimental observations (such as spectroscopic evidence of oxidation/reduction of the electrode material) are critically important to achieve further progress in SOFC design. Experimental characterization

* Corresponding author. E-mails: amasunov@mail.ucf.edu (A.E.M.); norlovsk@mail.ucf.edu (N.O.).
Received for review March 17, 2009 and accepted May 26, 2009
† Nanoscience Technology Center, University of Central Florida.
‡ Department of Chemistry, University of Central Florida.
§ Institute for Simulation and Training, University of Central Florida.
∥ Department of Physics, University of Central Florida.
⊥ Department of Mechanical, Materials and Aerospace Engineering, University of Central Florida.
DOI: 10.1021/am900182p
© 2009 American Chemical Society

techniques may not, however, always be available to determine certain properties and atomistic structure of the materials. In those cases, the computational investigation of the representative supercells from the first principles can greatly assist in completing the picture and achieve deeper understanding of the relevant processes. Such combined experimental and theoretical investigation has an added value and contributes to the design of more efficient and cost-effective devices.

The SOFC is built using porous solid ceramic cathode, anode, and dense electrolyte. The cathode is required to be stable in an oxidizing atmosphere, be electronically conductive, and maintain a porous structure at high operating temperatures. It is also beneficial for the cathode material to exhibit oxygen ion conductivity. To be a good oxygen ion conductor, a ceramic cathode should satisfy two fundamental requirements: (i) it has to contain a significant amount of vacancies in the oxygen sublattice, and (ii) the energy barriers for site to site oxygen migration need to be fairly small (3). Mixed ionic-electronic conducting transition metal perovskite type oxides are considered materials of choice for SOFC cathodes because of their porosity and good electrical conductivity.

Mixed oxides with the general formula ABO_3 crystallize in perovskite structure, where A cations are either lanthanides or alkaline earth metals, and B cations are transition metals such as Mn, Fe, or Co. These perovskites often have large mobility of the oxygen vacancies, exhibit strong ionic conductivity, and are often used as cathode materials in SOFC (1). The first studies of the mixed perovskite compounds were focused on lanthanum strontium cobaltite (LSC) with the formula $La_{1-x}Sr_xCoO_{3-\delta}$ (4). The high oxygen permeation flux in LSC was attributed to the high concentration of vacancy in the anion sublattice due to the substitution of La^{3+} by Sr^{2+} at the A-site of the perovskite (5). Unfortunately, at oxygen partial pressures <10 kPa and temperatures below 790 °C, LSC is unstable and phase transition to vacancy-ordered brownmillerite structure takes place. Burggraaf et al. examined oxygen permeability of perovskite-type oxides $SrCo_{0.8}B_{0.2}O_{3-\delta}$ (B = Cr, Fe, Co, and Cu) and $La_{0.6}Sr_{0.4}CoO_{3-\delta}$ (6). They found a 5 orders of magnitude increase in oxygen permeability (up to $0.3-3 \times 10^{-7}$ mol $cm^{-2}s^{-1}$) at the onset of the transition from a low-temperature vacancy-ordered state to defective perovskite for all compounds except $SrCo_{0.8}Fe_{0.2}O_{3-\delta}$. In the latter case, only a slight anomaly was found for the oxygen permeability. The comparatively high oxygen flux through $SrCo_{0.8}Fe_{0.2}O_{3-\delta}$ observed at intermediate temperatures was interpreted in terms of a two-phase mixture of a vacancy-ordered state and disordered perovskite, whereas above 790 °C, the sample is single-phase of defective perovskite structure (6). Kharton et al. measured oxygen permeation fluxes in $SrCo_{0.8}M_{0.2}O_3$ (M = Cr, Mn, Ni, Cu, Ti) materials using the electrochemical method (7, 8). The highest permeation flux was found for the strontium cobaltite-ferrite (SCF) perovskite with composition of $SrCo_{0.8}Fe_{0.2}O_3$. The substitution of Sr^{2+} ions in SCF by ions with higher charge such as La^{3+} usually increases phase stability, whereas the oxygen permeability is simultaneously decreasing (9, 10). Recently, a new solution to this permeability decrease was suggested. It consists of partial substitution of Sr^{2+} with Ba^{2+} in SCF. The resulting material, called barium−strontium cobaltite−ferrate (BSCF) has improved phase stability, whereas the oxygen permeation flux remains unchanged. Initially, BSCF was developed as a high-temperature oxygen permeation membrane material (5, 11). Recently Shao et al. proposed BSCF as an intermediate temperature cathode material (12). The reason of phase stability of BSCF is suggested by McIntosh et al. (13) According to their explanation, the Ba^{2+} ion is too large to sustain the transition-metal brownmillerite structure.

The size and charge of the B-site cations are found to be even more important parameters for the conductivity in perovskites. The B−O octahedra constitute the framework of the perovskite structure, and the oxide anion interacts with the B cation by a much stronger partially covalent bond, unlike the purely ionc bond to the large A cation. Lybye (14) compared four perovskites, $La_{0.9}Sr_{0.1}B_{0.9}Mg_{0.1}O_{2.9}$ (B = Al^{3+}, Ga^{3+}, Sc^{3+}, or In^{3+}) where only the B ion is changed, and found the maximum ionic conductivity for B = Ga^{3+}. This trend which could not be rationalized using the lattice free volume and the critical ionic radius point (proposed by Sammells et al. (15)) or by Goldschmidt factor points. Mogensen (16) rationalized the observed trend using the concept of the lattice stresses: a stress-free lattice will give the maximum oxide ion conductivity. The importance of the nature of the B-site ion is further evidenced by the results published on the rare earth gallates. Ishihara et al. (17) reported that substituting half of the Mg^{2+} in $La_{0.8}Sr_{0.2}Ga_{0.8}Mg_{0.2}O_{2.8}$ with Co or Ni ions improves the oxide ionic conductivity significantly. Another reason for improving ionic conductivity by different B-site cations is the change in concentration of the oxygen defects, tuned by substituting B-site cations with more or less reducible ones, or by substituting A-site cations with cations of a different charge (13).

In this paper, we report results of X-ray diffraction analysis, transmission electron microscopy, micro-Raman spectroscopy study, and density functional theory (DFT) calculations of structural and electronic properties of BSCF, including the spin states of B cations. Special attention is paid to the oxygen vacancies and cation ordering to clarify the stability of this material. Theoretical results are compared with experimental data.

2. EXPERIMENTAL AND COMPUTATIONAL DETAILS

$Ba_{0.5}Sr_{0.5}Co_{0.8}Fe_{0.2}O_3$ perovskite powder was synthesized by the solid-state reaction at NexTech Materials Inc. Its crystal structure was characterized by X-ray diffraction (XRD) analysis; microstructure was characterized by transmission electron microscopy (TEM), and vibrational response was analyzed by micro-Raman spectroscopy. XRD experiments were performed using an AXS-Bruker D8 Discover diffractometer with a Cu Kα X-ray radiation and Eurlean cradle. The lattice parameter of BSCF perovskite was refined using full profile analysis.

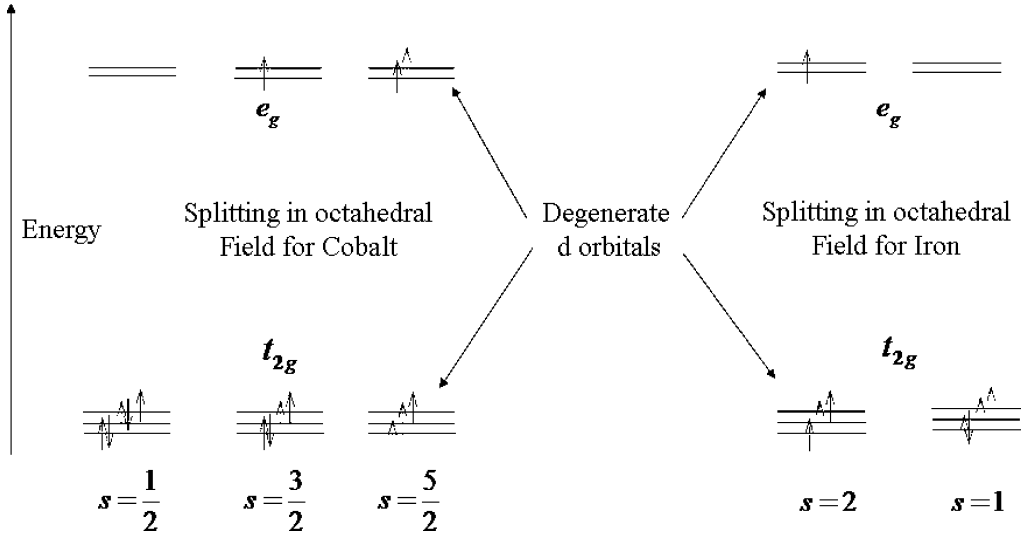

FIGURE 1. Different possible spin states of Fe^{4+} and Co^{4+} in octahedral crystal field.

Micro-Raman spectroscopy was used to characterize the vibrational properties of BSCF perovskite. Renishaw InVia Raman microscope was used to study the vibrational spectra of BSCF. The Raman microscope system comprises a laser (532 nm line of solid Si laser) to excite the sample, a single spectrograph fitted with holographic notch filters, and an optical microscope (a Leica microscope with a motorized XYZ stage) rigidly mounted and optically coupled to the spectrograph. The generated laser power was 25 mW. The average collection time for a single spectrum was 500 s. The incident and scattered beams were focused with a long working distance 50× objective, which allowed for keeping a laser spot as small as 2−3 μm. High-temperature experiments were performed using a TMS600 heating stage (Linkam Scientific Instruments Ltd., UK) by heating/cooling of the samples to/from 600 °C. The heating/cooling rate was 10 °C/min. Before BSCF measurements, the spectrometer was calibrated with a Si standard using a Si band position at 520.3 cm^{-1}. Renishaw Wire 2.0 software with a mixed Lorentzian and Gaussian peak fitting function was used to extract the peak's parameters.

All the calculations are based on the density functional theory (DFT) with the Perdew−Burke−Ernzerhof (PBE) exchange-correlation functional (18, 19) in the framework of Vanderbilt ultrasoft pseudopotentials (20) and plane wave basis set as it is implemented in Quantum-ESPRESSO program package (21). The Brillouine-zone integrations were performed using Monkhorst-Pack (22) grids using a 2 × 2 × 2 mesh for supercell calculations and 4 × 4 × 4 mesh for single unit. Spin-polarized calculation with fractional occupation numbers determined with Marzari-Vanderbilt cold smearing (23) and broadening factor of 0.04 Ry were used throughout. The geometry optimization was performed using Broyden-Fletcher-Goldfarb-Shanno algorithm (24). The wave function and electron density kinetic energy used the cutoffs of 45 and 360 Ry, respectively. We treated the Ba(5s,5p,6s), Sr(4s,4p,5s), Co(3d,4s), Fe(3d,4s), and O(2s,2p) electrons as valence states, while the remaining electrons were treated implicitly with core pseudopotentials. The Ba, Sr, and O pseudopotentials are obtained from pwscf pseudopotential library (25) and Co pseudopotentials were obtained from DACAPO pseudopotential library (26), whereas the Fe (3d,4s) pseudopotential was modified from existing pseudopotential (26). The existing pseudopotential (26) was describing valence electronic configuration as $3d^6 4s^1 4p^1$. We constructed the pseudopotential using the electron configuration as $3d^6 4s^2$ and used it in this study after validation.

Table 1. Calculated and Experimental Lattice Parameters *a* (Å) and Bulk Modulus *B* (GPa) of Pure Perovskites; ΔE is the Energy Difference with the Ground Spin State (kcal/mol)

		theoretical results (this work)			experimental results	
formula	spin state	*a* (Å)	*B* (GPa)	ΔE	*A* (Å)	*B* (GPa)
$SrCoO_3$	1/2	3.963		22.48		
	3/2	3.857		0.00	3.835[d]	
	5/2	3.825		7.45		
$SrFeO_3$	1	3.889		0.00	3.835[c]	
	2	3.847		9.604		
$BaTiO_3$		3.989	148.34		4.000[e]	135[a]
$SrTiO_3$		3.930	181.57		3.899[f]	179[b]

[a] See ref 35. [b] See ref 43. [c] See ref 44. [d] See ref 38. [e] See ref 45. [f] See ref 46

3. RESULTS AND DISCUSSION

In octahedral crystal field Co^{4+} can have three possible spin states, $t_{2g}^5 e_g^0$ ($s = 1/2$), $t_{2g}^4 e_g^1$ ($s = 3/2$), and $t_{2g}^3 e_g^2$ ($s = 5/2$) with one, three and five unpaired electrons, respectively. Fe^{4+} can have two possible spin states in the octahedral splitting with two and four unpaired electrons. These states have configurations as $t_{2g}^4 e_g^0$ ($s = 1$) and $t_{2g}^3 e_g^1$ ($s = 2$). We denote these states as low spin (LS) with one unpaired electron, intermediate spin (IS) with three unpaired electrons, and high spin (HS) states with five unpaired electrons for Co^{4+}, and as LS and HS states for Fe^{4+} cation according to their multiplicity. The spin-state configurations of Co^{4+} and Fe^{4+} in octahedral crystal field are schematically shown in Figure 1.

The accuracy of used pseudopotentials was validated by computing the equilibrium lattice parameter (a) for pure perovskites $SrCoO_3$, $SrFeO_3$, $BaTiO_3$, and $SrTiO_3$. For last two perovskites bulk moduli (B) were also calculated and compared with experimental values in Table 1. The bulk moduli were obtained by fitting the energy-volume curves using the Birch−Murnaghan equation of states (27). All calculations for the pure perovskites were performed using a unit cell containing a single formula unit. For modeling the mixed perovskite $Ba_{0.5}Sr_{0.5}Fe_{0.2}Co_{0.8}O_3$, we used a 2 × 2 × 2

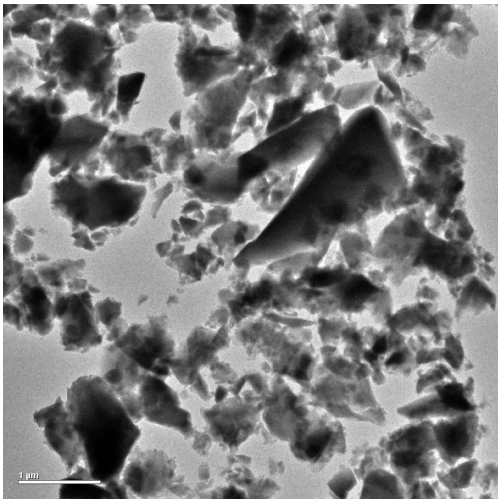

FIGURE 2. TEM micrograph showing a particle size and morphology of BSCF perovskite powder.

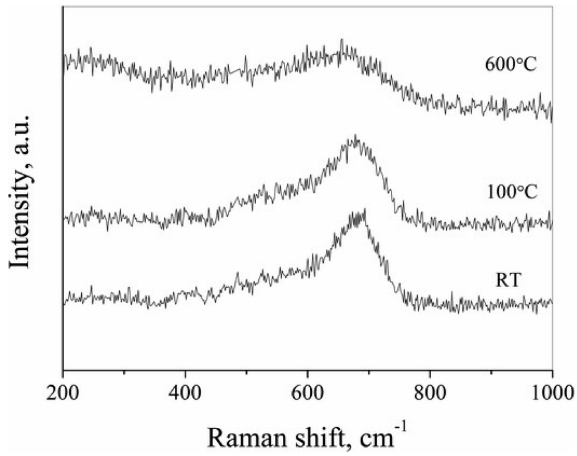

FIGURE 3. Raman spectra of BSCF indicates intensity decrease and broadening of ~675 cm^{-1} peak with elevated temperature.

supercell. One supercell has 4 Ba atoms, 4 Sr atoms, 2 Fe atoms, and 6 Co atoms, which results in a $Ba_{0.5}Sr_{0.5}Fe_{0.25}Co_{0.75}O_3$ formula unit, fairly close to the experimentally observed stoichiometry. For all investigated configurations, we calculated the Boltzmann factors at the temperature of sample preparation (1150 °C). These factors correspond to the frequency for each local structure occurring in the sample, assuming it was cooled down fast after the preparation. Annealing at lower temperatures is expected to increase the frequency for the more stable configurations and decrease the frequency for the less stable ones, whereas the relative order will remain the same.

The single phase BSCF perovskite was refined in cubic $Pm3m$ space group symmetry with a lattice constant a = 4.00013(8) Å. No secondary phases have been detected. The morphology and particle size of the BSCF are presented in Figure 2. As one can see, the powder particles have an irregular shape with a particle size of d_{50} = 0.35 μm. The chemical analysis using energy-dispersive spectrometer has shown the presence of Ba, Sr, Co, and Fe as well as oxygen atoms in the appropriate stoichiometry. Our observations are in agreement with the literature data. In a recent study on BSCF, the cubic phase was found to reversibly transform to a hexagonal polymorph upon long-term annealing at 900 °C (28). The phase stability of the cubic BSCF at higher temperature is confirmed by Yang et al. (29). According to their study, at 1000 °C, most of the compositions maintain the cubic phase.

In the ideal cubic perovskite structure, all lattice sites have inversion symmetry. Therefore, first-order Raman scattering is forbidden and no Raman active band is expected to be found in cubic BSCF perovskite (30). However, the broad band is detected at ~675 cm^{-1}, as is shown in Figure 3. This broad peak consists of the two overlapping bands which parameters, such as peak positions and intensities could be detected using the full width at half-maximum (FWHM) approach. The appearance of these vibration bands, forbidden in cubic structure, could be explained by the Jahn−Teller distortion in BSCF perovskite at room temperature. We associate this dynamic, local site distortion around the Co^{4+} cation with its intermediate spin state $t_{2g}^5e_g^1$. The presence of a single electron on the degenerate energy level results in distortion of the octahedral coordination of this cation by the first-order Jahn−Teller mechanism. The rising temperature will result in dynamic disorder, and average out the Jahn−Teller distortion. Thus, the intensities of the bands are expected to decrease, and the peaks become indistinguishable from the background. Therefore, the experimentally observed decrease in the intensities of two broad peaks at 600 °C reflects the transition to a dynamically less distorted local structure of BSCF.

In the case of the ordering of two different B-site cations in cubic perovskites a face-centered cubic superstructure with $Fm\bar{3}m$ symmetry is created (called elpasolite-type structure). This leads to several normal modes active in Raman spectra. Their wavenumbers were shown to change with temperature, whereas their intensities do not depend on the temperature significantly (31). Unlike the B-cation ordering, the Jahn−Teller distortion results in a strong temperature dependence of the Raman intensities, which was reported, for instance, in our previous study of $LaCoO_3$ (32), as well as other studies of this perovskite (33).

The comparisons of calculated and experimental values of lattice parameters and bulk modulus of pure perovskites are presented in Table 1. In agreement with experimental data (34), our calculations result in IS state of the cobalt ion for the ground state of $SrCoO_3$. For this compound, our calculations also demonstrate a close agreement with the experimental value of the lattice parameter (35) (the deviation is +0.2 % for LS state, and −0.6 % for IS state, whereas the deviation is as large as 3.3 % for HS state). The IS state of Co^{3+} was experimentally observed with photoemission spectra (36) and the ferromagnetic resonance measurements (37). The experimental value for magnetic moment of strontium cobaltite $SrCoO_3$ is 2.1 μ_B. This value of magnetic moment is bracketed by idealized magnetic moments of HS and LS states (38). Our calculations give the total

energies for LS and HS states to be 7.46 and 22.48 kcal/mol above the IS state.

In the case of $SrFeO_3$ compound, we found the HS state to be more stable by 9.60 kcal/mol compared to LS state, which is also consistent with experiment (36). The calculated lattice parameter for both LS and HS states deviates from the experimental value (39) by −0.2 and −1.3%, respectively. From the Table 1, we can conclude that the ground electronic spin state of Co^{3+} in $SrCoO_3$ is IS, whereas Fe in $SrFeO_3$ has HS ground state.

For the model BSCF supercell, we performed optimization of the lattice parameter corresponding to the ambient zero pressure. Experiments show (12), that the oxygen sublattice of BSCF in nonstoichiometric and molar fraction of the oxygen vacancies is $\delta = 0.38$ at 1150 °C. To address this fact, we studied the relative stability of the oxygen deficient supercells with respect to various vacancy positions. Structures with up to 4 oxygen vacancies per supercell were considered. They correspond to the formula $Ba_{0.5}Sr_{0.5}Co_{0.8}Fe_{0.2}O_{3-\delta}$ with $\delta = 0.125$, 0.25, 0.375, and 0.5. The calculated lattice parameter was found to be within 0.3% from the experimental lattice parameter of BSCF for all concentrations of vacancies. This result is in agreement with the neutron diffraction study performed by McIntosh et.al (40).

To determine the spin state of the supercell, two spin states for Fe ($s = 1$ and $s = 2$) were combined with three spin states for Co^{4+} ($s = 1/2$, $s = 3/2$, and $s = 5/2$). According to experimental data, the $SrFe_{1-x}Co_xO_3$ compound is antiferromagnetic for $x < 0.10-0.15$ and becomes ferromagnetic for $x \geq 0.2$ (41). The ferromagnetic state of $SrFeO_3$ was also found to be the most stable at LSDA+U level of theory (42). On the basis of these data, we considered Fe and Co cations in BSCF supercell to be ferromagnetically coupled.

The spin state of the transition metal ions in BSFC was examined by Löwdin population analysis. The results of this analysis for $SrCoO_3$ and $SrFeO_3$ perovskite structures at different spin states reveal ferromagnetic coupling between transition metal cations. Herein we tested all the examined structures by Löwdin population analysis in order verify the spin states of individual cations and their ferromagnetic ordering in structures under investigation.

To determine the most stable spin state of the stoichiometric BSCF, we combined one of the two possible spin states for Fe^{4+} cation with one of the three spin states for Co^{4+}. Our calculated results are presented in Table 2 and demonstrate that the ground state of the BSCF supercell without defects is formed by IS state of Co^{4+} and HS state of Fe^{4+}. This is the most stable state with Boltzmann factor of 98%. For this ground state, the structural relaxation of the supercell converges to the structure with tetragonal distortion around the Co^{4+} cation, shown in Figure 4. This result is in agreement with the experimentally observed Jahn−Teller lattice distortion of BCSF, discussed above. Because both elongation and contraction of Co−O interionic distances are observed in simultaneous fashion, overall symmetry of the structure remains cubic as shown in Figure 4. This theoretical conclusion is reinforced by experimental Raman spectroscopy data shown in Figure 3, where the decrease of the intesity of a broad peak ~675 cm^{-1} occurs at elevated temperatures and complete disappearance of the peak is expected as temperature rises further. The existence of IS state of Co^{3+} ion is also observed experimentally in different lanthanum-based cobaltites (32, 43, 44).

Table 2. Relative Ground State Energies of $Ba_{0.5}Sr_{0.5}Co_{0.8}Fe_{0.2}O_3$ with Different Spin States on Fe and Co Cations and *C* Denotes Boltzmann Factor Calculated at 1150 °C

spin states on Fe and Co cations (S_{Fe}, S_{Co})	relative ground-state energy (kcal mol^{-1})	*C* (%)
(1,3/2)	9.66	2
(2,3/2)	0.00	98
(1,5/2)	35.23	0
(2,5/2)	101.37	0

The model supercell without vacancies can have nine inequivalent arrangements of Fe^{4+} and Co^{4+} cations at the B positions as well as Ba^{2+} and Sr^{2+} cations in A positions. The relative stability for all of these structures are listed in Table 3, where the relative positions of cations are labeled according to Figure 5. From the Boltzmann factor in the last column in Table 3, one can clearly see that there is no preferred cation arrangement. Thus, we conclude that the transition metal cations fill their positions almost randomly.

All four different oxygen vacancy concentrations mentioned above were examined. On the first step of the simulation, we varied different ionic positions in the defect free supercell. On the second step, we randomly removed

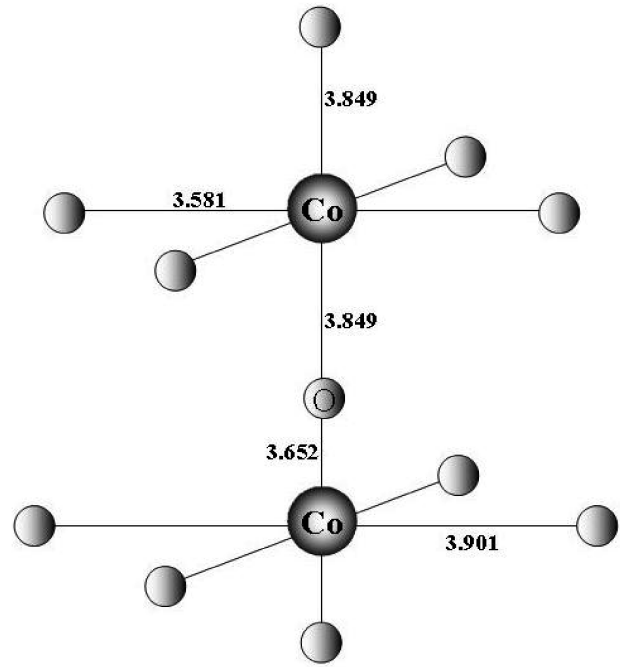

FIGURE 4. Jahn−Teller distortion of coordination octahedron around of Co^{4+} cation at the intermediate spin state in BSCF supercell. Calculated equilibrium distances between Co^{4+} and nearest oxygen ions are labeled.

Table 3. Relative Ground State Energies of BSCF Supercell with Respect to Different Cation Positions; Index for Cations Indicates the Positions According to Figure 5, and Spin States are $S = 2$ (Fe), $S = 3/2$ (Co); ΔE is the Relative Ground State Energy (kcal/mol), C indicates the BoltzmannFactors at 1150 °C

Fe1	Fe2	Co1	Co2	Co3	Co4	Co5	Co6	Ba1	Ba2	Ba3	Ba4	Sr1	Sr2	Sr3	Sr4	ΔE	C
1	5	2	3	4	6	7	8	10	11	13	16	9	12	14	15	2.03	8
1	6	2	3	4	5	7	8	10	11	13	16	9	12	14	15	2.01	8
1	8	2	3	4	5	6	7	10	11	13	16	9	12	14	15	2.54	6
1	5	2	3	4	6	7	8	10	12	14	16	9	11	13	15	0.00	18
1	6	2	3	4	5	7	8	10	12	14	16	9	11	13	15	0.10	18
1	8	2	3	4	5	6	7	10	12	14	16	9	11	13	15	0.76	13
1	5	2	3	4	6	7	8	11	12	13	14	9	10	15	16	1.42	10
1	6	2	3	4	5	7	8	11	12	13	14	9	10	15	16	1.41	10
1	8	2	3	4	5	6	7	11	12	13	14	9	10	15	16	1.95	8

one oxygen atom from the most stable stoichiometric configuration and calculated the relative energy of oxygen vacant supercells. The results are collected in Table 4. As one can see, the first vacancy prefers to stay between Fe and Co (or two Co ions), whereas the second vacancy favors the coordination octahedron of the Co atom neighboring the first vacancy. The third vacancy favors the other coordination octahedron, involved in the first vacancy. There it has two preferred positions: in cis-position to the second vacancy (L-shaped vacancy trimer), or in trans-position to it (linear vacancy trimer). The vacancy ordering into the linear chains is observed during phase transition from disordered cubic perovskites to the brownmillerite phases of $ABO_{2.5}$ stoichiometry. In our calculations, the L-shaped vacancy trimer was found to be more stable than the linear vacancy with significantly higher Boltzmann factor, shown in the last column of Table 4. The four vacancy positions obtained after removing the fourth oxygen atoms are shown in Figure 6.

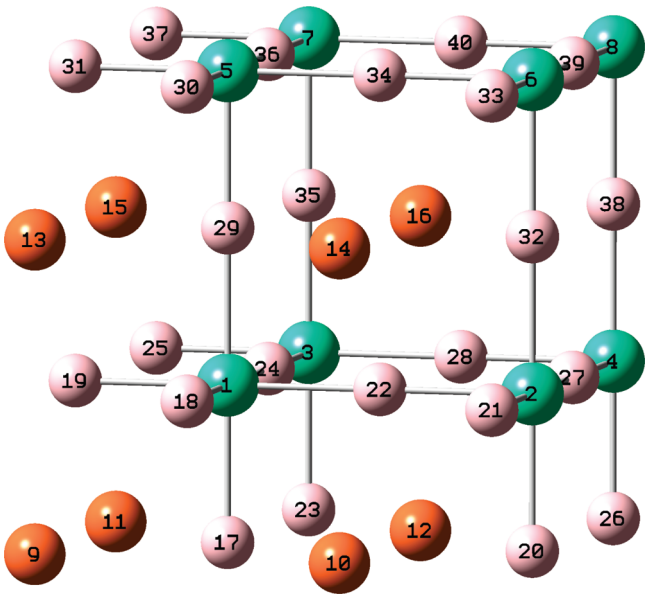

FIGURE 5. ABO_3 perovskite supercell used for calculation. Sites B (iron or cobalt cations) represented using indexes 1−8, sites A (barium or strontium cations) represented using indexes 9−16, while indexes 17−40 represent Oxygen ions.

Table 4. Relative Ground-State Energies ΔE (kcal/mol) of 1, 2, 3, and 4-Oxygen-Deficient $Ba_{0.5}Sr_{0.5}Co_{0.8}Fe_{0.2}O_{3-\delta}$ Supercells with Respect to Different Vacancy Positions (denoted according to Figure 5); Positions of Cations are Fe = 1,5; Co = 2,3,4,6,7,8; Ba = 10,12,14,16; Sr = 9,11,13,15 (see Figure 5)

V_1	V_2	V_3	V_4	ΔE (kcal/mol)	C (%) at 1150 °C
29				6.24	7
24				0	67
35				3.13	21
22				11.06	1
27				7.92	4
24	18			19.47	0
24	22			7.72	3
24	28			4.88	9
24	29			3.15	17
24	32			6.08	6
24	34			11.30	1
24	35			0.00	54
24	36			9.81	2
24	38			6.49	5
24	39			10.39	1
24	40			10.47	1
24	35	17		10.07	2
24	35	23		5.02	11
24	35	33		11.16	1
23	24	29		3.88	17
23	24	36		0.00	69
23	24	29	30	4.59	9
23	24	35	26	10.87	1
24	29	35	36	0.00	47
24	29	18	17	0.23	43

The most stable vacancy tetramer configuration is a square. Thus, our calculations found the linear vacancy ordering to be unfavorable compared to the tetrameric islands of vacancies. This is in agreement with the experimental fact that the BSCF structure remains cubic in the observed oxygen deficiency range whereas the similar Ba-free compound forms brownmillerite structure with linear vacancy ordering (13). The formation of two, three, and four oxygen vacancies in BSCF supercell changes the coordination of two, three, or four transition metal cations, adjacent to the vacancy. Formation of square vacancy tetramer changes the ideal octahedron coordination of four transition metal ions into the distorted tetrahedron. Its relaxed geometry is shown in Figure 6.

4. CONCLUSIONS

In the present study, we combine the experimental characterization of doped BSCF perovskite of the formula $Ba_{0.5}Sr_{0.5}Co_{0.8}Fe_{0.2}O_{3-\delta}$ with plane wave DFT calculations. The homogeneous phase composition and cubic structure with 4.0012 Å lattice parameter was confirmed by X-ray diffraction analysis, transmission electron microscopy, and microphotographs. The Jahn−Teller distortion of octahedral coordination around Co^{4+} cations was observed experimentally and explained theoretically. The calculations show that

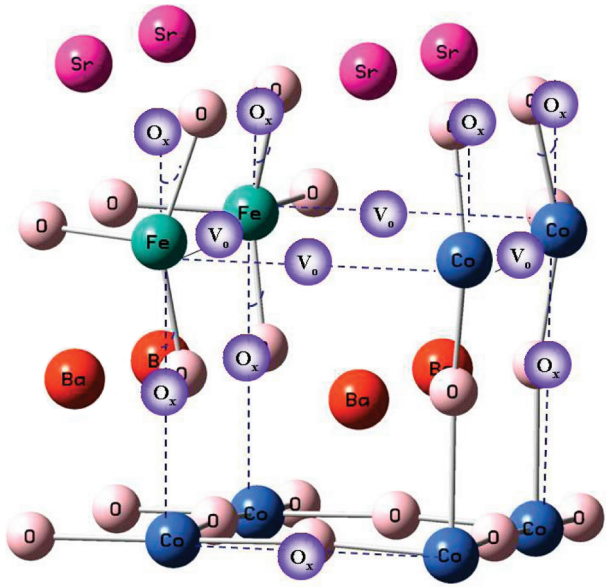
Sr
Sr
Sr
Sr
Fe
Fe
Co
Co
Co
Co
Co
Co
Ba
Ba
B
B
O
O
O

(39) Watanabe, *J. Phys. Soc. Jpn.* **1957**, *12*, 515.
(40) McIntosh, S.; Vente, J. F.; Haije, W. G.; Blank, D. H. A.; Bouwmeester, H. J. M. *Chem. Mater.* **2006**, *18*, 2187–2193.
(41) Lee, K. W.; Pickett, W. E. *Phys. Rev. B: Condens. Matter Mater. Phys* **2006**, *73*, 174428–8.
(42) Shein, I. R.; Shein, K. I.; Kozhevnikov, V. L.; Ivanovskii, A. L. *Phys. Solid State* **2005**, *47*, 2082–2088.
(43) Wang, Z. L.; Zhang, J. *Phys. Rev. B: Condens. Matter Mater. Phys* **1996**, *54*, 1153.
(44) Yamaguchi, S.; Okimoto, Y.; Tokura, Y. *Phys. Rev. B: Condens. Matter Mater. Phys* **1997**, *55*, R8666.
(45) Lheureux, D.; Fischer, M.; Polian, A.; Itie, J. P.; Gauthier, M.; Syfosse, G. *Proc. IEEE Ultrasonics Symp.* **1999**, 533–536.
(46) Takeda, T. *J. Phys. Soc. Jpn.* **1972**, *33*, 967.
(47) *Ternary Compounds, Organic Semiconductors*; Springer: New York, 2000; Vols. I. H. I. E., pp 1−6.
(48) Abramov, Y. A.; Tsirelson, V. G.; Zavodnik, V. E.; Ivanov, S. A.; Brown, I. D. *Acta Crystallogr., Sect. B* **1995**, *51*, 942–951.

AM900182P